



Quantifying the snowmelt-albedo feedback at Neumayer Station, East Antarctica

Constantijn L. Jakobs¹, Carleen H. Reijmer¹, Peter Kuipers Munneke¹, Gert König-Langlo², and Michiel R. van den Broeke¹

¹Institute for Marine and Atmospheric Research Utrecht, Utrecht University, Utrecht, The Netherlands

²Alfred-Wegener-Institut Helmholtz-Zentrum für Polar- und Meeresforschung, Bremerhaven, Germany

Correspondence: Stan Jakobs (c.l.jakobs@uu.nl)

Abstract. We quantify the snowmelt-albedo feedback at Neumayer Station, East Antarctica, using 24 years (1992–2016) of high-quality meteorological observations to force a surface energy balance model. The modelled 24-year cumulative surface melt at Neumayer amounts to 1060 mm water equivalent (w.e.), with only a small uncertainty (± 3 mm w.e.) from random measurement errors. Results are more sensitive to the chosen value for the surface momentum roughness length and fresh snow density, yielding a range of 800–1140 mm w.e. Melt at Neumayer occurs only in the months November to February, with a summer average of 46 mm w.e. and large interannual variability ($\sigma = 40$ mm w.e.). Absorbed shortwave radiation is the dominant driver of temporal melt variability at Neumayer. To assess the importance of the melt-albedo feedback we include and calibrate an albedo parameterisation in the surface energy balance model. We show that, without the snowmelt-albedo feedback, surface melt at Neumayer would be approximately three times weaker, demonstrating how important it is to correctly represent this feedback in model simulations of surface melt.

1 Introduction

The Antarctic ice sheet (AIS) contains more than 25 million km³ of ice, sufficient to raise global mean sea level by almost 60 m if melted completely (Fretwell et al., 2013). Between 1992 and 2017, the AIS lost mass at an accelerated rate, contributing 7.6 \pm 3.9 mm to global sea level (Shepherd et al., 2018). This mass loss is mainly observed in coastal West Antarctica and the Antarctic Peninsula (AP), and is caused by glaciers that accelerated after their buttressing ice shelves thinned or disintegrated (Wouters et al., 2015; Turner et al., 2017). The interaction between meltwater and firn, the intermediate product between snow and glacier ice, is hypothesised to play an important role in ice shelf disintegration (Kuipers Munneke et al., 2014). If the firn layer contains enough air, as is the case for most of the AIS, meltwater can percolate downwards and refreeze (Ligtenberg et al., 2014). If the storage capacity of the firn layer is reduced, surface meltwater can flow laterally towards the ice shelf edge (Bell et al., 2017), be stored englacially (Lenaerts et al., 2017) or form ponds on the ice shelf surface (Kingslake et al., 2017). In all cases, meltwater can accumulate in crevasses, thereby increasing the hydrostatic pressure in the crevasse tip, causing it to penetrate farther down. When a crevasse reaches the bottom of the ice shelf or a basal crevasse, part of the ice shelf disintegrates, a process called hydrofracturing (Van der Veen, 2007). Hydrofracturing has been identified as a potential precursor for rapid



loss of Antarctic ice, accelerating sea level rise (DeConto and Pollard, 2016). In combination with enhanced ocean swell under low sea-ice conditions (Massom et al., 2018), hydrofracturing caused the disintegration of Larsen B ice shelf in the AP in 2002 (Rignot et al., 2004; Scambos et al., 2004). In July 2017, a large iceberg calved from Larsen C ice shelf, but it is unclear whether this signifies a further southward progression of ice shelf destabilisation in the AP (Hogg and Gudmundsson, 2017).

5 Improving our predictive capabilities of future ice shelf stability, AIS mass loss and associated sea level rise, thus requires a thorough understanding of the surface melt process on Antarctic ice shelves. In contrast to meltwater occurrence, which is readily observed from space (Picard et al., 2007; Tedesco, 2009; Luckman et al., 2014), observational estimates of surface melt rates on Antarctic ice shelves are rare; they have been obtained locally through explicit modelling of the surface energy balance (SEB) (Van den Broeke et al., 2010; Kuipers Munneke et al., 2012, 2018), which enabled continent-wide melt estimates using 10 calibrated satellite products (Trusel et al., 2013, 2015). These studies invariably demonstrate that in most parts of Antarctica, melt currently is a weak and intermittent process. In this melt regime, the positive snowmelt-albedo feedback plays a decisive role: when snow melts, meltwater may refreeze in the cold snow pack, resulting in considerably larger grains (~ 1 mm) than fresh snow or snow that has been subjected to dry compaction (~ 0.1 mm). Larger snow grains enhance forward scattering of photons into the snowpack, increasing the probability of absorption, reducing the surface albedo especially in the near-infrared 15 (Wiscombe and Warren, 1980; Gardner and Sharp, 2010). This further enhances absorption of solar radiation and melt. For pure, uncontaminated snow, the strength of the snowmelt-albedo feedback depends on multiple factors, e.g., the intensity and duration of the melt and the frequency and intensity of snowfall events, which provide new snow consisting of smaller grains. We therefore expect the snowmelt-albedo feedback to be spatially and temporally variable on Antarctic ice shelves.

Most studies on the snowmelt-albedo feedback address the disappearance of (seasonal) snow and the surfacing of dark 20 soil/open water (Perovich et al., 2002; Hall, 2004; Flanner et al., 2007; Qu and Hall, 2007), leading to further warming of the air/water. These studies commonly express the melt-albedo feedback in terms of air/water temperature sensitivity. Our aim is to quantify the impact on the melt rate of the darkening but not the disappearance of snow, a process addressed by far fewer 25 studies (Box et al., 2012; Van As et al., 2013). To that end, we implement a snow albedo parameterization (Gardner and Sharp, 2010; Kuipers Munneke et al., 2011b) in an SEB model, which is then calibrated using observations and used to study the sensitivity of melt rates to snow properties that influence snow albedo. We use 24 years of high-quality in situ observations (König-Langlo, 2017) from the German research station Neumayer (Fig. 1) to calculate the SEB and melt rate. We investigate the effects of measurement uncertainties and model settings on the calculated cumulative amount of surface melt. We then analyse the main drivers of surface melt and the magnitude of the snowmelt-albedo feedback at Neumayer by switching on/off different components of the albedo parameterisation.

30 The SEB model is explained in Sect. 2.1, followed by a description of the albedo parameterisation in Sect. 2.2. The meteorological data used to force the SEB model are described in Sect. 2.3, in Sect. 3 we present and discuss the modelled SEB and in Sect. 4 we present the impact of the snowmelt-albedo feedback on the melt. Finally, the results are briefly discussed in Sect. 5.



2 Methods

2.1 Surface Energy Balance model

The energy balance model is a further development of the models presented by Reijmer et al. (1999), Reijmer and Oerlemans (2002) and Kuipers Munneke et al. (2012); here only the main features are described. The energy balance of an infinitesimally thin surface layer (the ‘skin’ layer) is defined as:

$$M = SW \downarrow + SW \uparrow + LW \downarrow + LW \uparrow + Q_S + Q_L + Q_G \quad (1)$$

where positive fluxes are defined to be directed towards the surface. $SW \downarrow$ and $SW \uparrow$ are the incoming and reflected shortwave radiation, $LW \downarrow$ and $LW \uparrow$ are the downward and upward longwave radiation, Q_S and Q_L the turbulent sensible and latent heat fluxes and Q_G is the conductive subsurface heat flux. We neglect latent energy from rain. M is the energy used to melt snow or ice, and is non-zero only when the surface has reached the melting point ($T_0 = 273.15$ K). In order to calculate Q_G and allow for densification, meltwater percolation and refreezing, a snow/firn model with initially 52 layers is used. The layer thickness varies from 4 cm at the top to 2 m at the bottom, and the lowermost level is at 25 m depth. Here, we impose a no-flux boundary condition. Fresh snow density is parameterised following the expression of Lenaerts et al. (2012), which relates it to the prevailing surface temperature (T_s) and 10 m wind speed (V_{10m}) and imposes a lower limit of fresh snow density $\rho_{s,0}$. Meltwater percolation is based on the tipping-bucket method (e.g. Ligtenberg et al., 2011), allowing for immediate downward transport (within a single timestep of 50 s) of remaining water if a layer has attained its maximum capillary retention, as modelled using the expressions of Schneider and Jansson (2004). Meltwater refreezing increases the density and temperature of a layer. At the bottom of the firn layer, the meltwater is assumed to run off immediately, i.e. the model does not allow for slush/superimposed ice formation or lateral water movement. The calculation of the turbulent fluxes is based on Monin-Obukhov similarity theory between a single measurement level (2 m for temperature and humidity, 10 m for wind) and the surface, assuming the latter to be saturated with respect to ice and using the stability functions according to Dyer (1974) for unstable and Holtslag and De Bruin (1988) for stable conditions. Penetration of shortwave radiation into the snow is not taken into account. This might underestimate melt since shortwave radiation warms the near-surface snow pack more rapidly than the ground heat flux alone would (Kuipers Munneke et al., 2009). However, as subsurface temperature measurements at Neumayer are very scarce, the evaluation of the modelled penetration of shortwave radiation is infeasible.

The terms in Eq. (1) are either based on observations or can be expressed as a function of the skin temperature T_s . The SEB is solved iteratively by looking for a value of T_s that closes the SEB to within 0.005 K between iterations: if $T_s > 273.15$ K, it is reset to 273.15 K and excess energy is used for surface melt M . To evaluate model performance, the modelled value of T_s is compared to observed T_s calculated from $LW \uparrow$, using Stefan-Boltzmann’s law

$$LW \uparrow = \sigma \epsilon T_s^4, \quad (2)$$

where $\sigma = 5.67 \cdot 10^{-8} \text{ W m}^{-2} \text{ K}^{-4}$ is the Stefan-Boltzmann constant and ϵ the longwave emissivity of the surface, which is set to 1.



2.2 Albedo parameterisation

Conventionally, incoming shortwave radiation ($SW \downarrow$) is prescribed to the surface energy balance model from the radiation observations. However, in order to investigate the feedbacks of the snow properties on albedo and melt (Sect. 4), we instead calculate $SW \downarrow$ from measured $SW \uparrow$ by an albedo parameterisation based on properties of the snow (Gardner and Sharp, 2010;

- 5 Kuipers Munneke et al., 2011b). As rime formation could possibly affect the observation of $SW \downarrow$, we decided to parameterise $SW \downarrow$ and use $SW \uparrow$ to assess model performance (Van den Broeke et al., 2004).

The parameterised surface albedo α is described as a base albedo α_S , modified by perturbations describing the effect of changing solar zenith angle θ ($d\alpha_u$), the cloud optical thickness τ ($d\alpha_\tau$) and the concentration of black carbon in the snow ($d\alpha_c$):

$$10 \quad \alpha = \alpha_S + d\alpha_u + d\alpha_\tau + d\alpha_c. \quad (3)$$

For Antarctica, we neglect the impact of impurities in the snow ($d\alpha_c = 0$); $d\alpha_u$ and $d\alpha_\tau$ both depend on the base albedo α_S , $d\alpha_u$ in addition depends on the solar zenith angle ($u = \cos \theta$), and $d\alpha_\tau$ on the cloud optical thickness τ :

$$d\alpha_u = 0.53\alpha_S(1 - \alpha_S)(1 - 0.64x - (1 - x)u)^{1.2}, \quad (4)$$

$$d\alpha_\tau = \frac{0.1\tau(\alpha_S + d\alpha_c)^{1.3}}{(1 + 1.5\tau)^{\alpha_S}}, \quad (5)$$

15 where $x = \min\left(\frac{\sqrt{\tau}}{3u}, 1\right)$. The base albedo depends on the snow grain size r_e (in m):

$$\alpha_S = 1.48 - 1.27048r_e^{0.07}, \quad (6)$$

in which the snow grain size r_e on time step t is parameterised as

$$r_e(t) = [r_e(t-1) + dr_{e,dry} + dr_{e,wet}]f_o + r_{e,0}f_n + r_{e,r}f_r. \quad (7)$$

Here $dr_{e,dry}$ and $dr_{e,wet}$ describe the metamorphism of dry and wet snow respectively, f_o , f_n and f_r are the fractions of old, 20 new and refrozen snow, and $r_{e,0}$ and $r_{e,r}$ are the grain sizes of fresh and refrozen snow. $dr_{e,wet}$ is a function of the snow grain size r_e itself and the liquid water content f_{liq} (Brun et al., 1989):

$$dr_{e,wet} = \frac{C f_{liq}^3}{4\pi r_e^2}, \quad (8)$$

where C is a constant ($4.22 \cdot 10^{-13} \text{ m}^3 \text{ s}^{-1}$). The calculation of the dry snow metamorphism ($dr_{e,dry}$ in Eq. (7)) uses a look-up table consisting of values for the dry snow metamorphism for different fresh snow grain sizes and as a function of



snow temperature, temperature gradient and snow density. The fractions f_o , f_n and f_r are derived from the snow/firn model, and the grain sizes of fresh and refrozen snow are constants; the method for determining their values from a tuning exercise is described in Sect. 4.1.

To determine cloud optical thickness τ , an empirical relation between τ and the longwave-equivalent cloud cover N_ϵ is used
5 following Kuipers Munneke et al. (2011a):

$$\tau = c_1 (\exp(c_2 N_\epsilon) - 1), \quad (9)$$

with fit parameters c_1 and c_2 . N_ϵ is determined using a method described by Kuipers Munneke et al. (2011a) which relates hourly values of downward longwave radiation $LW \downarrow$ to near-surface air temperature T_{2m} as illustrated in Fig. 2a. Red lines indicate quadratic fits through the upper and lower 5 percentile of the data, assuming to represent fully cloudy and clear conditions, respectively. N_ϵ is obtained by linearly interpolating between these upper and lower bounds, yielding values between 0 and 1. Hourly values for cloud cover are then used to obtain values for τ (Fig. 2b). The values used for the fit parameters $c_1 = 5.404$ and $c_2 = 2.207$ (both dimensionless) differ somewhat from Kuipers Munneke et al. (2011a), who used daily values for the fit.

2.3 Observational data

15 The SEB model is forced with data from the meteorological observatory at the German research station Neumayer, situated on the Ekström ice shelf (König-Langlo, 2017). The observatory has been operational since 1981, and was relocated in 1992 and 2009. The current location is $70^{\circ}40'S$, $8^{\circ}16'W$ (Fig. 1). The observatory is one of only four Antarctic stations –and the only one situated on an ice shelf– that is part of the Baseline Surface Radiation Network (BSRN), a global network of stations with high-quality radiation observations, coordinated by the Alfred Wegener Institute (AWI). The meteorological variables used in this study and their uncertainty ranges are provided in Table 1. We use hourly averages of 2 m temperature (T_{2m}) and specific humidity (q_{2m}), 10 m wind speed (V_{10m}), surface pressure (p) and radiation fluxes for the period April 1992–January 2016 (24 years) to force the SEB model. Approximately 4.1% of the data points contained at least one missing variable, which mostly come from daily performed visual validation processes. To obtain a continuous data set all missing data were replaced: pressure, relative humidity, wind speed, temperature and longwave radiation were simply linearly interpolated. In case of shortwave radiation, the missing value was replaced by imitating the average daily cycle of the two preceding days. As the measurement station is visited and maintained every day, the impact of rime formation is limited, as is tilt of the observation mast, resulting in a high-quality meteorological data set.

Accumulation observations are only available from stake measurements, performed weekly for the period April 1992–January 2009. As timing of precipitation is important for correctly simulating the effects of fresh snow on snow albedo, 30 we combined the stake observations with precipitation predicted by the regional atmospheric climate model RACMO2.3p2 (Van Wessem et al., 2018) to obtain realistic timing of precipitation in between stake observations, as well as for the post-2009



period. The amount of precipitation modelled by RACMO2 was scaled such that the modelled surface height changes agrees with stake measurements; this required a 15.3% upward adjustment of the modelled precipitation flux.

3 Results: near surface climate, surface energy balance and melt

3.1 SEB model performance and uncertainties

5 There are several SEB model parameters for which the exact values or formulations are unknown, e.g., the surface roughness lengths, the density of fresh snow ρ_s , the stability functions (required to calculate the turbulent scales) and the effective conductivity, which couples the magnitude of Q_G to the temperature gradient in the snow. We estimated the impact of observational and model uncertainties on modelled melt by running the model 600 times while randomly varying all hourly observations within the specified measurement uncertainty ranges (Table 1) and using multiple expressions for the heat conductivity and
10 stability functions. Model performance is quantified by comparing modelled with observed T_s and assessing the changes in 24-year total cumulative melt.

The choice of expressions for the stability functions and heat conductivity did not significantly impact the modelled amount of melt (total within 30 mm w.e. or 2.7 %, not shown). The model outcomes are more sensitive to the choice of surface roughness length for momentum $z_{0,m}$ and the lower limit of density of fresh snow $\rho_{s,0}$ (Fig. 3). When $z_{0,m}$ is varied between
15 0.5 mm and 50 mm and $\rho_{s,0}$ between 150 and 500 kg m⁻³, the cumulative amount of surface melt over the 24-year period varies between 800 – 1140 mm w.e., with higher melt values for smaller values of $z_{0,m}$ and $\rho_{s,0}$. Our interpretation of this result is that decreasing $z_{0,m}$ and $\rho_{s,0}$ decreases the turbulent fluxes as well as Q_G , reducing the efficiency at which heat is removed from the surface, allowing more energy to be invested in melt. The sensitivity to $z_{0,m}$ is somewhat unexpected, because by using the formulations proposed by Andreas (1987), both $z_{0,h}$ and $z_{0,q}$ decrease for increasing $z_{0,m}$, which acts to dampen the
20 effect on the magnitude of the turbulent fluxes.

Optimal values in terms of simulated T_s are $z_{0,m} = 2.0$ mm and $\rho_{s,0} = 320$ kg m⁻³, resulting in a T_s bias of 0.01 K and an RMSD of 0.78 K (Fig. 4). We use these values in the remainder of this study. The value for $z_{0,m}$ is high compared to the values found during a field campaign in 1982 (König, 1985); the values presented here should therefore not be regarded as best estimates for the actual values, they merely resemble parameters that yield the best comparison with observations. Measured
25 values of T_s in excess of the melting point in Fig. 4 reflect uncertainties in the adopted unit value of longwave emissivity and in measured $LW \uparrow$, e.g. from sensor window heating (Smeets et al., 2018).

Figure 5 shows modelled 24-year cumulative melt at Neumayer and uncertainties associated with measurement errors (red coloured band) and model parameters (blue coloured band). The total melt amounts to 1060 mm w.e., with a small uncertainty associated with measurement uncertainties ($1\sigma \approx 3$ mm w.e., i.e. 0.3 %). The adopted method to estimate this uncertainty has
30 its limitations, as measurement errors are probably autocorrelated: if a measurement at one time is disturbed in some way, it is probably disturbed in a similar way at the next time step. Therefore, this result could be interpreted as a lower bound of the uncertainty range, which is supported by the larger uncertainty estimates (~15%) by Van den Broeke et al. (2010), who applied a constant systematic error which can be interpreted as an upper bound on the modelled uncertainty range. This



also explains why the uncertainties deriving from the choice of $z_{0,m}$ are so much larger: these runs represent prescribing a systematic error between the true (unknown) value and the chosen value, assuming the true value to be constant, which likely is an oversimplification (Smeets and Van den Broeke, 2008).

3.2 Near surface climate

5 Neumayer station is located on a flat ice shelf approximately 22 km from Halvfarryggen ice rise to the southeast, ~100 km from the ice shelf break (grounding line) to the south and ~20 km from open water to the north and ~5 km to open water to the east. As a result, Neumayer experiences relatively mild conditions without significant impact from katabatic winds but with a pronounced influence of synoptic low-pressure systems passing mainly from west to east in the south Atlantic Ocean to the north of the station. Figure 6a shows the period averaged (1993–2015) seasonal cycles of 2 m air temperature (T_{2m}),
10 specific humidity (q_{2m}) and 10 m wind speed (V_{10m}), the bands indicating the standard deviation of the monthly means. Summer temperatures around -4°C and winter temperatures around -25°C imply a substantial (>20 K) seasonal temperature amplitude based on monthly mean values. This is in line with the formation of a surface-based temperature inversion in winter, a phenomenon that is representative for the flat ice shelves as well as the interior ice domes and in contrast to the topographically steeper escarpment zone, where the quasi-continuous mixing by katabatic flow limits the formation of such an
15 inversion (Van den Broeke, 1998). Interannual variability in T_{2m} and V_{10m} is largest in austral winter, indicative of the regular disruption of the surface temperature inversion by advection of warm, cloudy air and strong synoptic winds associated with the passage of low-pressure systems, which are most active in non-summer months due to the larger equator-to-pole temperature difference (Van Loon, 1967). As expected from the strong link to the air temperature through the Clausius-Clapeyron relation and a high annual mean relative humidity of 82 % because of the proximity of a saturated snow surface and the ocean, the
20 seasonal cycle of q_{2m} closely follows that of temperature. Highest wind speeds are from the east (Fig. 7) and almost no northerly winds (between approximately 340 and 20 degrees) are observed. This supports the findings by Klöwer et al. (2013), who attributed the absence of northerly winds to the fact that most low-pressure systems pass to the north of Neumayer at several degrees latitude distance. Furthermore, they showed that fluctuations in wind speed and direction are primarily a result of synoptic-scale systems.

25 3.3 Surface energy balance

Timeseries of annual (Mar–Feb) mean near-surface meteorological quantities and SEB components are presented in Fig. 8, with annual mean values in Table 2 and seasonal cycles presented in Fig. 6b. The annual mean values for year X are obtained by averaging monthly values for March of year X until February of year $X + 1$. Table 2 and Fig. 8 both show that the SEB is dominated by the radiation fluxes; in spite of the high albedo of the snow surface, SW_{net} is the dominant heat source for the
30 skin layer in summer. LW_{net} extracts energy from the surface, most efficiently so in summer when the surface is heated by the sun. In summer, Q_L becomes a significant heat loss in the SEB (sublimation), preventing strong negative Q_S (convection). The seasonal cycle of Q_G is small, indicating a small net transport of heat away from the surface in summer and towards the



surface in winter. The net annually integrated amount is less than zero as a result of the refreezing of meltwater, warming the subsurface snow layers.

Significant and previously unreported trends are detected in $LW \uparrow (-0.39 \pm 0.12 \text{ W m}^{-2} \text{ yr}^{-1})$ and $Q_S (+0.24 \pm 0.08 \text{ W m}^{-2} \text{ yr}^{-1})$, both a result of wintertime trends. $LW \uparrow$ is linked directly to T_s , which also shows a negative trend ($-0.05 \pm 0.02 \text{ K yr}^{-1}$),
5 which in magnitude exceeds the negative trend in T_{2m} ($-0.02 \pm 0.02 \text{ K yr}^{-1}$), the probability that the negative trend in T_s is greater in magnitude than the trend in T_{2m} is 0.86). As a result, the temperature gradient near the surface has increased, enhancing Q_S . The negative trend in T_s originates from a decrease in $LW \downarrow (-0.35 \pm 0.16 \text{ W m}^{-2} \text{ yr}^{-1})$, which is in turn driven by a slight decrease in cloud cover ($-0.004 \pm 0.001 \text{ yr}^{-1}$). This is suggested independently by the decrease in average winter humidity ($-0.004 \pm 0.002 \text{ g kg}^{-1} \text{ yr}^{-1}$). These findings agree with Herman et al. (2013), who determined from satellite
10 observations that summer cloud cover has decreased over that part of coastal Antarctica in the period 1979–2011. The negative temperature trend is consistent with findings by Schmittüsen et al. (2015), who show that an increase in atmospheric CO_2 tends to cool the atmosphere over Antarctica.

3.4 Melt season

Melt occurs at Neumayer from November until February (Fig. 9), but is highly variable from year to year. The mean annual
15 amount of melt is 46 mm w.e. with an interannual variability of 40 mm w.e. and a range of 2 mm w.e. in 1999–2000 to 161 mm w.e. in 2012–13. Most melt occurs in December and January and the surface only sporadically reaches the melting point in February. Only in 2007 did melt occur in November, and no melt occurs outside these four months. The cumulative melt occurring at Neumayer shows sharp increases (Fig. 5), which indicate the peaked melt seasons, in which melt occurs on average on 19 ± 9 days, with a melt day defined as a day with non-zero melt. The uncertainty in the number of melt days due to the
20 chosen values of $z_{0,m}$ and $\rho_{s,0}$ is relatively small compared to the interannual variability in melt totals (Fig. 9), implying that this choice does not significantly affect the modelled melt duration, but it does affect the total melt.

To investigate the link between melt and climate, we compare the two summers with the highest (2003–04 and 2012–13, on average 134 mm w.e.) and lowest (1999–2000 and 2014–15, on average 2 mm w.e.) melt amounts. Figure 10 shows the meteorological and SEB components for these years, averaged over December and January. The largest differences are
25 found in T_{2m} (+2.0 K) and SW_{net} (+17 W m^{-2}); based on the measurement uncertainties, these differences are significant. In cold summers, the low T_{2m} corresponds to a stronger temperature inversion ($T_{2m} - T_s$), more longwave cooling, less sublimation and a larger Q_S . The difference in SW_{net} is caused solely by surface albedo, which suggests an important role for the snowmelt-albedo feedback. This will be elaborated upon in the next section. Finally, the direction of Q_G is reversed; in high melt years, the surface is warmed from below while in low melt years the surface loses heat to the subsurface. More
30 refreezing of meltwater in high melt years warms the near surface snow layers, which in turn leads to a conductive heat flux towards the surface.



4 Results: the snowmelt-albedo feedback

The snowmelt-albedo feedback is a well-known phenomenon, but has not before been quantified for Antarctica. The feedback occurs after the sudden growth of snow grains when meltwater penetrates into the subsurface and refreezes. Because a photon on average travels farther through snow with large particles than in fresh snow with smaller particles, the probability of it being absorbed is increased, effectively lowering the surface albedo (Gardner and Sharp, 2010). Even without melt, albedo decreases when snow ages, following grain growth from dry snow metamorphism, but this is a much slower process which mainly depends on temperature gradients in the snow, favouring moisture transport onto larger grains. To quantify the snowmelt-albedo feedback at Neumayer, we implemented the albedo parameterisation described in Sect. 2.2 in the SEB model and optimised its performance by maximising the correspondence between 1) modelled and observed hourly $SW \uparrow$, and 2) the total melt obtained from the calculations based on observed albedo (Sect. 4.1). We compare $SW \uparrow$ in stead of the albedo itself because in this case the hourly values are naturally weighted with its contribution to S_{net} and hence its importance for the SEB. We then perform several runs with different processes affecting the surface albedo to investigate the importance of the snowmelt-albedo feedback for melt at Neumayer (Sect. 4.2).

4.1 Optimising the albedo parameterisation

The albedo parameterisation, and especially the expression for snow grain size (Eq. (7)) contains several parameters that are not well constrained, such as fresh snow grain size $r_{e,0}$ and refrozen snow grain size $r_{e,r}$. These parameters were varied within reasonable ranges to optimise the results. The best comparison with observed albedo was achieved when using the look-up table for dry snow metamorphism $dr_{e,dry}$ corresponding to a grain size of $54.5 \mu\text{m}$. However, it was found that for this value of the fresh snow grain size, the metamorphism of dry snow was still too slow. A factor was introduced to scale the dry snow metamorphism, and used as a third parameter to optimise the albedo parameterisation.

The first step in optimising the parameterisation was to split the summer season into two parts, the ‘dry’ and the ‘wet’ season. The respective starts of the dry and wet seasons are the first day on which the sun rises more than 15° above the horizon and the first day that surface melt occurs ($M > 0 \text{ mm w.e.}$). The wet season ends when the sun no longer rises higher than 15° . For the dry season, we varied the dry snow metamorphism factor and the fresh snow grain size to best match observed $SW \uparrow$ (Fig. 11). This resulted in a fresh snow grain size of $198 \mu\text{m}$ and a scale factor for dry snow metamorphism of 1.293. These values are then used in the second step, in which the refrozen snow grain size $r_{e,r}$ is varied to best match the cumulative melt using observed albedo. This was achieved for a refrozen snow grain size of 1.55 mm . This is compatible with the typical largest grains in dry metamorphosed snow of $O(1 \text{ mm})$, and which Kuipers Munneke et al. (2011b) used as a lower limit for refrozen snow grains.

For these values the model adequately reproduces the incoming shortwave radiation (Fig. 12, bias = $+0.74 \text{ W m}^{-2}$, RMSD = 7.4 W m^{-2}), providing confidence in the modelled albedo.



4.2 Magnitude of the snowmelt-albedo feedback

With these parameters settings, three experiments with the SEB model were carried out in addition to the original run (R_0) which uses the measured albedo:

- R_1 : the average measured albedo (0.84, determined by adding all $SW \downarrow$ and $SW \uparrow$ for all measurements when the Sun is higher than 15° above the horizon and taking the ratio between the two) is prescribed for the entire period;
- R_2 : the full albedo parameterisation is used;
- R_3 : refrozen snow does not contribute to the changing snow characteristics, i.e. $f_r = 0$ in Eq. (7).

Figure 13a and b show time series of cumulative and seasonal surface melt for the four experiments. Run R_1 underpredicts melt in most seasons, yielding a mean annual amount of surface melt of 36 ± 27 mm w.e. yr^{-1} (c.f. 46 ± 40 mm w.e. yr^{-1} of run R_0). More melt was modelled in the 1995–96 melt season, which was characterised by frequent precipitation events and cloudy conditions, keeping observed albedo higher than the long-term mean. This result motivates the need for an albedo parameterisation. The run using the full albedo parameterisation (R_2) adequately reproduces the amount of seasonal melt (46 ± 37 mm w.e. yr^{-1}), although melt in e.g. the 2012 melt season is underestimated. Run R_3 represents the situation in which the snowmelt-albedo feedback has been switched off, leading to significantly underpredicted melt (16 ± 14 mm w.e. yr^{-1}).

Defining the strength of the snowmelt-albedo feedback (SMAF) as the ratio between the total seasonal surface melt in experiments R_2 and R_3 , we obtain an average value of 2.8, with a range of 1.1 (1994–1995) to 5.8 (2010–11, see Fig. 13c). Propagating the uncertainties leads to uncertainties in the determination of the SMAF of typically 12%, with a range of 2% (1995–96) to 43% (2006–07), which allows for the determination of a significant trend in Fig. 13c of $+0.07 \pm 0.02$ per year ($p < 0.001$). Significant but weak correlations were found between SMAF and cloud cover ($R^2 = 0.14$, $p = 0.08$), $SW \downarrow$ ($R^2 = 0.13$, $p = 0.09$) and the interval between precipitation events ($R^2 = 0.19$, $p = 0.04$). The first two can be related to each other: fewer clouds allow for more insolation, thus increasing $SW \downarrow$. The observed correlation between SMAF and the intervals between precipitation is related to the structure of the snow/firn layer. The longer the interval between precipitation events, the longer it takes before the surface albedo is ‘reset’ by fresh snow and the higher the impact of the snowmelt-albedo feedback. Significant but rather weak correlations were found as well between SMAF and the mean surface temperature of the preceding winter season (July–October, $R^2 = 0.15$, $p = 0.07$), $LW \uparrow$ of the preceding winter season (July–October, $R^2 = 0.18$, $p = 0.04$) and the total precipitation of the preceding winter season (September–October, $R^2 = 0.13$, $p = 0.09$). However, these correlations have the opposite sign of what would be expected: an increase in precipitation would act as an extra buffer for the snow layer, delaying the moment of exposing a lower albedo snow layer. Similarly, a colder snow surface would contain smaller grain sizes and hence have a higher albedo. In future studies we will focus on the temporal and spatial variability of SMAF and we shall further investigate these trends and their causes.

If SMAF would be defined as the ratio between R_0 and R_3 , the observed trend would disappear or even change sign. Defining SMAF this way makes the signal more prone to noise due to the performance of the albedo parameterisation itself, as the result no longer solely stems from the difference in the way surface albedo is calculated. For example in 1994–95 there is a large



discrepancy between R_0 and R_2 , resulting in a much higher SMAF if it were defined with respect to measured albedo. We believe defining SMAF as the ratio between R_2 and R_3 is more reliable as those runs only differ in which processes contribute to the surface albedo.

5 Conclusions

5 In this study, we used 24 years of high-quality meteorological and radiation observations from the BSRN station Neumayer, situated on Ekström ice shelf, East Antarctica, to force a surface energy balance model. The primary goal was to calculate the amount of melt at Neumayer and to investigate the importance of the snowmelt-albedo feedback. Model performance was evaluated based on the difference between modelled and measured surface temperature, and the calculated melt was tested for measurement and model parameter uncertainties. We found that measurement uncertainties, when considered random in time, 10 do not significantly impact modelled melt at Neumayer (<0.5 % difference). However, melt amount and model performance are sensitive to the values chosen for the surface roughness length for momentum $z_{0,m}$ and lower limit of fresh snow density $\rho_{s,0}$, thus accurate measurements of these values would further improve future modelling studies. Our results confirm that melt at Neumayer is an intermittent process, occurring on average on only 19 days each summer, totalling 46 mm w.e. and with an interannual variability of 40 mm w.e. Melt occurs mainly in December and January, sporadically in February and only 15 once melt was modelled in November. Significant and previously unreported trends were found in the net longwave radiation (decreasing) and the sensible heat flux (increasing), but these are unrelated to the melt at Neumayer as they mainly occur in winter and are attributed to a decrease in cloud cover.

The main difference between high and low melt years was found to be surface albedo, implying an important role for the snowmelt-albedo feedback (SMAF). We quantified SMAF by implementing and tuning an albedo parameterisation in the 20 SEB model, which includes the effects of fresh snowfall and wet and dry snow metamorphism on albedo. SMAF on average enhances surface melt at Neumayer by a factor of 2.8 ± 1.2 , the uncertainty allowing for a trend analysis ($+0.07 \pm 0.02$ per year). Correlations were found in SMAF with cloud cover, $SW \downarrow$ and the gaps between precipitation events, though they were all rather weak; to assess how the importance of the melt-albedo feedback may vary spatially and temporally, the next step in this research will be applying this method to a regional climate model (Van Wessem et al., 2018)).

25 *Code and data availability.* The Neumayer data is available upon request via the website of AWI (<https://bsrn.awi.de/data/data-retrieval-via-pangaea/>).
The model output is available upon request by the authors.

Author contributions. CLJ performed the study and wrote the manuscript. PKM assisted with the implementation of the albedo parameterisation. GKL was in charge of the Neumayer data. CHR, PKM, GKL and MRvdB have commented on the manuscript,



Competing interests. The authors declare no competing interests.

Acknowledgements. We would like to thank the AWI for maintaining the station and the Baseline Surface Radiation Network (BSRN) for providing the data, with special thanks to Amelie Driemel for creating a citation reference and Holger Schmithüsen for helping to interpret the data. C.L. Jakobs and C.H. Reijmer acknowledge support from the Netherlands Polar Programme under project number 866.15.204.



References

- Andreas, E. L.: A theory for the scalar roughness and the scalar transfer coefficients over snow and sea ice, *Boundary-Layer Meteorology*, 38, 159–184, <https://doi.org/10.1007/BF00121562>, 1987.
- Bell, R. E., Chu, W., Kingslake, J., Das, I., Tedesco, M., Tinto, K. J., Zappa, C. J., Frezzotti, M., Boghosian, A., and Lee, W. S.: Antarctic ice shelf potentially stabilized by export of meltwater in surface river, *Nature*, 544, 344–348, <https://doi.org/10.1038/nature22048>, 2017.
- Box, J. E., Fettweis, X., Stroeve, J. C., Tedesco, M., Hall, D. K., and Steffen, K.: Greenland ice sheet albedo feedback: thermodynamics and atmospheric drivers, *The Cryosphere*, 6, 821–839, <https://doi.org/10.5194/tc-6-821-2012>, 2012.
- Brun, E., Martin, E., Simon, V., Gendre, C., and Coléou, C.: An Energy and Mass Model of Snow Cover Suitable for Operational Avalanche Forecasting, *Journal of Glaciology*, 35, 333–342, <https://doi.org/10.3189/S002214300009254>, 1989.
- DeConto, R. M. and Pollard, D.: Contribution of Antarctica to past and future sea-level rise, *Nature*, 531, 591–597, <https://doi.org/10.1038/nature17145>, 2016.
- Dyer, A. J.: A review of flux-profile relationships, *Boundary-Layer Meteorology*, 7, 363–372, <https://doi.org/10.1007/BF00240838>, 1974.
- Flanner, M. G., Zender, C. S., Randerson, J. T., and Rasch, P. J.: Present-day climate forcing and response from black carbon in snow, *Journal of Geophysical Research*, 112, <https://doi.org/10.1029/2006JD008003>, 2007.
- Fretwell, P., Pritchard, H. D., Vaughan, D. G., Bamber, J. L., Barrand, N. E., Bell, R. E., Bianchi, C., Bingham, R. G., Blankenship, D. D., Casassa, G., Catania, G., Callens, D., Conway, H., Cook, A. J., Corr, H. F. J., Damaske, D., Damm, V., Ferraccioli, F., Forsberg, R., Fujita, S., Gim, Y., Gogineni, P., Griggs, J. A., Hindmarsh, R. C. A., Holmlund, P., Holt, J. W., Jacobel, R. W., Jenkins, A., Jokat, W., Jordan, T., King, E. C., Kohler, J., Krabill, W., Riger-Kusk, M., Langley, K. A., Leitchenkov, G., Leuschen, C., Luyendyk, B. P., Matsuoka, K., Mouginot, J., Nitsche, F. O., Nogi, Y., Nost, O. A., Popov, S. V., Rignot, E., Rippin, D. M., Rivera, A., Roberts, J., Ross, N., Siegert, M. J., Smith, A. M., Steinhage, D., Studinger, M., Sun, B., Tinto, B. K., Welch, B. C., Wilson, D., Young, D. A., Xiangbin, C., and Zirizzotti, A.: Bedmap2: improved ice bed, surface and thickness datasets for Antarctica, *The Cryosphere*, 7, 375–393, <https://doi.org/10.5194/tc-7-375-2013>, 2013.
- Gardner, A. S. and Sharp, M. J.: A review of snow and ice albedo and the development of a new physically based broadband albedo parameterization, *Journal of Geophysical Research: Earth Surface*, 115, <https://doi.org/10.1029/2009JF001444>, 2010.
- Hall, A.: The Role of Surface Albedo Feedback in Climate, *Journal of Climate*, 17, 1550–1568, [https://doi.org/10.1175/1520-0442\(2004\)017<1550:TROSAF>2.0.CO;2](https://doi.org/10.1175/1520-0442(2004)017<1550:TROSAF>2.0.CO;2), 2004.
- Herman, J., DeLand, M. T., Huang, L.-K., Labow, G., Larko, D., Lloyd, S. A., Mao, J., Qin, W., and Weaver, C.: A net decrease in the Earth's cloud, aerosol, and surface 340 nm reflectivity during the past 33 yr (1979–2011), *Atmospheric Chemistry and Physics*, 13, 8505–8524, <https://doi.org/10.5194/acp-13-8505-2013>, 2013.
- Hogg, A. E. and Gudmundsson, G. H.: Impacts of the Larsen-C Ice Shelf calving event, *Nature Climate Change*, 7, 540–542, <https://doi.org/10.1038/nclimate3359>, 2017.
- Holtslag, A. A. M. and De Bruin, H. A. R.: Applied Modeling of the Nighttime Surface Energy Balance over Land, *Journal of Applied Meteorology*, 27, 689–704, [https://doi.org/10.1175/1520-0450\(1988\)027<0689:AMOTNS>2.0.CO;2](https://doi.org/10.1175/1520-0450(1988)027<0689:AMOTNS>2.0.CO;2), 1988.
- Kingslake, J., Ely, J. C., Das, I., and Bell, R. E.: Widespread movement of meltwater onto and across Antarctic ice shelves, *Nature*, 544, 349–352, <https://doi.org/10.1038/nature22049>, 2017.



Klöwer, M., Jung, T., König-Langlo, G., and Semmler, T.: Aspects of weather parameters at Neumayer station, Antarctica, and their representation in reanalysis and climate model data, *Meteorologische Zeitschrift*, 22, 699–709, <https://doi.org/10.1127/0941-2948/2013/0505>, 2013.

König, G.: Roughness Length of an Antarctic Ice Shelf, *Polarforschung*, 55, 27–32, <https://doi.org/10.2312/polarforschung.55.1.27>, 1985.

5 König-Langlo, G.: Basic and other measurements, and meteorological synoptical observations from Neumayer Station, 1992-04 to 2016-01, reference list of 572 datasets, <https://doi.pangaea.de/10.1594/PANGAEA.874984>, 2017.

Kuipers Munneke, P., Van den Broeke, M. R., Reijmer, C. H., Helsen, M. M., Boot, W., Schneebeli, M., and Steffen, K.: The role of radiation penetration in the energy budget of the snowpack at Summit, Greenland, *The Cryosphere*, 3, 155–165, <https://doi.org/10.5194/tc-3-155-2009>, 2009.

10 Kuipers Munneke, P., Reijmer, C. H., and Van den Broeke, M. R.: Assessing the retrieval of cloud properties from radiation measurements over snow and ice, *International Journal of Climatology*, 31, 756–769, <https://doi.org/10.1002/joc.2114>, 2011a.

Kuipers Munneke, P., Van den Broeke, M. R., Lenaerts, J. T. M., Flanner, M. G., Gardner, A. S., and Van de Berg, W. J.: A new albedo parameterization for use in climate models over the Antarctic ice sheet, *Journal of Geophysical Research: Atmospheres*, 116, <https://doi.org/10.1029/2010JD015113>, 2011b.

15 Kuipers Munneke, P., Van den Broeke, M. R., King, J. C., Gray, T., and Reijmer, C. H.: Near-surface climate and surface energy budget of Larsen C ice shelf, *Antarctic Peninsula*, *The Cryosphere*, 6, 353–363, <https://doi.org/10.5194/tc-6-353-2012>, 2012.

Kuipers Munneke, P., Ligtenberg, S. R. M., Van den Broeke, M. R., and Vaughan, D. G.: Firn air depletion as a precursors of Antarctic ice-shelf collapse, *Journal of Glaciology*, 60, 205–214, <https://doi.org/10.3189/2014JoG13J183>, 2014.

20 Kuipers Munneke, P., Luckman, A. J., Bevan, S. L., Smeets, C. J. P. P., Gilbert, E., Van den Broeke, M. R., Wang, W., Zender, C. S., Hubbard, B., Ashmore, D., Orr, A., King, J. C., and Kulessa, B.: Intense Winter Surface Melt on an Antarctic Ice Shelf, *Geophysical Research Letters*, 45, <https://doi.org/10.1029/2018GL077899>, 2018.

Lenaerts, J. T. M., Van den Broeke, M. R., Déry, S. J., Van Meijgaard, E., Van de Berg, W. J., Palm, S. P., and Sanz Rodrigo, J.: Modeling drifting snow in Antarctica with a regional climate model: 1. Methods and model evaluation, *Journal of Geophysical Research: Atmospheres*, 117, <https://doi.org/10.1029/2011JD016145>, 2012.

25 Lenaerts, J. T. M., Lhermitte, S., Drews, R., Ligtenberg, S. R. M., Berger, S., Helm, V., Smeets, C. J. P. P., Van den Broeke, M. R., Van de Berg, W. J., Van Meijgaard, E., Eijkelboom, M., Eisen, O., and Pattyn, F.: Meltwater produced by wind-albedo interaction stored in an East Antarctic ice shelf, *Nature Climate Change*, 7, 58–62, <https://doi.org/10.1038/nclimate3180>, 2017.

Ligtenberg, S. R. M., Helsen, M. M., and Van den Broeke, M. R.: An improved semi-empirical model for the densification of Antarctic firn, *The Cryosphere*, 5, 809–819, <https://doi.org/10.5194/tc-5-809-2011>, 2011.

30 Ligtenberg, S. R. M., Kuipers Munneke, P., and Van den Broeke, M. R.: Present and future variations in Antarctic firn air content, *The Cryosphere*, 8, 1711–1723, <https://doi.org/10.5194/tc-8-1711-2014>, 2014.

Luckman, A., A., E., Jansen, D., Kulessa, B., Kuipers Munneke, P., King, J. C., and Barrand, N. E.: Surface melt and ponding on Larsen C Ice Shelf and the impact of föhn winds, *Antarctic Science*, 26, 625–635, <https://doi.org/10.1017/S0954102014000339>, 2014.

35 Massom, R. A., Scambos, T. A., Bennetts, L. G., Reid, P. A., Squire, V. A., and Stammerjohn, S. E.: Antarctic ice shelf disintegration triggered by sea ice loss and ocean swell, *Nature*, 558, 383–389, <https://doi.org/10.1038/s41586-018-0212-1>, 2018.

Perovich, D. K., Grenfell, T. C., Light, B., and Hobbs, P. V.: Seasonal evolution of the albedo of multiyear Arctic sea ice, *Journal of Geophysical Research*, 107, <https://doi.org/10.1029/2000JC000438>, 2002.



- Picard, G., Fily, M., and Gallee, H.: Surface melting derived from microwave radiometers: a climatic indicator in Antarctica, *Annals of Glaciology*, 46, 29–34, <https://doi.org/10.3189/172756407782871684>, 2007.
- Qu, X. and Hall, A.: What Controls the Strength of Snow-Albedo Feedback?, *Journal of Climate*, 20, 3971–3981, <https://doi.org/10.1175/JCLI4186.1>, 2007.
- 5 Reijmer, C. H. and Oerlemans, J.: Temporal and spatial variability of the surface energy balance in Dronning Maud Land, East Antarctica, *Journal of Geophysical Research*, 107, <https://doi.org/10.1029/2000JD000110>, 2002.
- Reijmer, C. H., Greuell, W., and Oerlemans, J.: The annual cycle of meteorological variables and the surface energy balance on Berkner Island, Antarctica, *Annals of Glaciology*, 29, 49–54, <https://doi.org/10.3189/172756499781821166>, 1999.
- Rignot, E., Casassa, G., Gogineni, P., Krabill, W., Rivera, A., and Thomas, R.: Accelerated ice discharge from the Antarctic Peninsula 10 following the collapse of Larsen B ice shelf, *Geophysical Research Letters*, 31, <https://doi.org/10.1029/2004GL020697>, 2004.
- Scambos, T. A., Bohlander, J. A., Shuman, C. A., and Skvarca, P.: Glacier acceleration and thinning after ice shelf collapse in the Larsen B embayment, Antarctica, *Geophysical Research Letters*, 31, <https://doi.org/10.1029/2004GL020670>, 2004.
- Schmithüsen, H., Notholt, J., König-Langlo, G., Lemke, P., and Jung, T.: How increasing CO₂ leads to an increased negative greenhouse effect in Antarctica, *Geophysical Research Letters*, 42, 10 422–10 428, <https://doi.org/10.1002/2015GL066749>, 2015.
- 15 Schneider, T. and Jansson, P.: Internal accumulation in firn and its significance for the mass balance of Storglaciären, Sweden, *Journal of Glaciology*, 50, 25–34, <https://doi.org/10.3189/172756504781830277>, 2004.
- Shepherd, A., Ivins, E. R., Rignot, E., Smith, B., Van den Broeke, M. R., Velicogna, I., Whitehouse, P. L., Briggs, K. H., Jougin, I., Krinner, G., Nowicki, S., Payne, A. J., Scambos, T. A., Schlegel, N., A. G., Agosta, C., Ahlstrøm, A. P., Babonis, G., Barletta, V. R., Blazquez, A., Bonin, J., Csatho, B., Cullather, R. I., Felikson, D., Fettweis, X., Forsberg, R., Gallee, H., Gardner, A. S., Gilbert, L., Groh, A., Gunter, B., Hanna, E., Harig, C., Helm, V., Horvath, A., Horwath, M., Khan, S., Kjeldsen, K. K., Konrad, H., Langen, P., Lecavalier, B., Loomis, B., Lutcke, S. B., McMillan, M., Melini, D., Mernild, S., Mohajerani, Y., Moore, P., Mouginot, J., Moyano, G., Muir, A., Nagler, T., Nield, G., Nilsson, J., Noël, B. P. Y., Otosaka, I., Pattle, M. E., Peltier, W. R., Pie, N., Rietbroek, R., Rott, H., Sandberg Sørensen, L., Sasgen, I., Save, H., Scheuchl, B., Schrama, E. J. O., Schröder, L., Seo, K.-W., Simonsen, S., Slater, T., Spada, G., Sutterly, T. C., Talpe, M., Tarasov, L., Van de Berg, W. J., Van der Wal, W., Van Wessem, J. M., Vishwakarma, B. D., Wiese, D., and Wouters, B.: Mass balance 20 of the Antarctic Ice Sheet from 1992 to 2017, *Nature*, 558, 219–222, <https://doi.org/10.1038/s41586-018-0179-y>, 2018.
- Smeets, C. J. P. P. and Van den Broeke, M. R.: Temporal and Spatial Variations of the Aerodynamic Roughness Length in the Ablation Zone 25 of the Greenland Ice Sheet, *Boundary-Layer Meteorology*, 128, 315–338, <https://doi.org/10.1007/s10546-008-9291-0>, 2008.
- Smeets, C. J. P. P., Kuipers Munneke, P., Van As, D., Van den Broeke, M. R., Boot, W., Oerlemans, J., Snellen, H., Reijmer, C. H., and Van de 30 Wal, R. S. W.: The K-transect in west Greenland: Automatic weather station data (1993–2016), *Arctic, Antarctic, and Alpine Research*, 50, <https://doi.org/10.1080/15230430.2017.1420954>, 2018.
- Tedesco, M.: Assessment and development of snowmelt retrieval algorithms over Antarctica from K-band spaceborn brightness temperature (1979–2008), *Remote Sensing of Environment*, 113, 979–997, <https://doi.org/10.1016/j.rse.2009.01.009>, 2009.
- Trusel, L. D., Frey, K. E., Das, S. B., Kuipers Munneke, P., and Van den Broeke, M. R.: Satellite-based estimates of Antarctic surface meltwater fluxes, *Geophysical Research Letters*, 40, 6148–6153, <https://doi.org/10.1002/2013GL058138>, 2013.
- 35 Trusel, L. D., Frey, K. E., Das, S. B., Karnauskas, K. B., Kuipers Munneke, P., Van Meijgaard, E., and Van den Broeke, M. R.: Divergent trajectories of Antarctic surface melt under two twenty-first-century climate scenarios, *Nature Geoscience*, 8, 927–934, <https://doi.org/10.1038/NGEO2563>, 2015.



Turner, J., Orr, A., Gudmundsson, G. H., Jenkins, A., Bingham, R. G., Hillenbrand, C.-D., and Bracegirdle, T. J.: Atmosphere-ocean-ice interactions in the Amundsen Sea Embayment, West Antarctica, *Reviews of Geophysics*, 55, 235–276, <https://doi.org/10.1002/2016RG000532>, 2017.

Van As, D., Fausto, R. S., Colgan, W. T., Box, J. E., Ahlstrøm, A. P., Andersen, S. B., Andersen, M. L., Charalampidis, C., Citterio, M.,
5 Edelvang, K., Jensen, T. S., Larsen, S. H., Machguth, H., Nielsen, S., Veicherts, M., and Weidick, A.: Darkening of the Greenland ice sheet due to the melt-albedo feedback observed at PROMICE weather stations, *Geological Survey of Denmark and Greenland Bulletin*, 28, 69–72, 2013.

Van den Broeke, M. R.: The semi-annual oscillation and Antarctic climate. Part 1: influence on near surface temperatures (1957–79), *Antarctic Science*, 10, 175–183, <https://doi.org/10.1017/S0954102098000248>, 1998.

10 Van den Broeke, M. R., Reijmer, C. H., and Van de Wal, R. S. W.: Surface radiation balance in Antarctica as measured with automatic weather stations, *Journal of Geophysical Research*, 109, <https://doi.org/10.1029/2003JD004394>, 2004.

Van den Broeke, M. R., König-Langlo, G., Picard, G., Kuipers Munneke, P., and Lenaerts, J. T. M.: Surface energy balance, melt and sublimation at Neumayer Station, East Antarctica, *Antarctic Science*, 22, 87–96, <https://doi.org/10.1017/S0954102009990538>, 2010.

Van der Veen, C. J.: Fracture propagation as means of rapidly transferring surface meltwater to the base of glaciers, *Geophysical Research Letters*, 34, <https://doi.org/10.1029/2006GL028385>, 2007.

Van Loon, H.: The Half-Yearly Oscillations in Middle and High Southern Latitudes and the Coreless Winter, *Journal of the Atmospheric Sciences*, 24, 472–486, [https://doi.org/10.1175/1520-0469\(1967\)024<0472:THYOIM>2.0.CO;2](https://doi.org/10.1175/1520-0469(1967)024<0472:THYOIM>2.0.CO;2), 1967.

Van Wessem, J. M., Van de Berg, W. J., Noël, B. P. Y., Van Meijgaard, E., Birnbaum, G., Jakobs, C. L., Krüger, K., Lenaerts, J. T. M.,
20 Lhermitte, S., Ligtenberg, S. R. M., Medley, B., Reijmer, C. H., Van Tricht, K., Trusel, L. D., Van Ulf, L. H., Wouters, B., Wuite, J., and Van den Broeke, M. R.: Modelling the climate and surface mass balance of polar ice sheets using RACMO2, part 2: Antarctica (1979–2016), *The Cryosphere*, 12, 1479–1498, <https://doi.org/10.5194/tc-2017-202>, 2018.

Wiscombe, W. J. and Warren, S. G.: A Model for the Spectral Albedo of Snow. I: Pure Snow, *Journal of the Atmospheric Sciences*, 37, 2712–2733, [https://doi.org/10.1175/1520-0469\(1980\)037<2712:AMFTSA>2.0.CO;2](https://doi.org/10.1175/1520-0469(1980)037<2712:AMFTSA>2.0.CO;2), 1980.

Wouters, B., Martin-Español, A., Helm, V., Flament, T., Van Wessem, J. M., Ligtenberg, S. R. M., Van den Broeke, M. R., and Bamber, J. L.,
25 Dynamic thinning of glaciers on the Southern Antarctic Peninsula, *Science*, 348, 899–903, <https://doi.org/10.1126/science.aaa5727>, 2015.

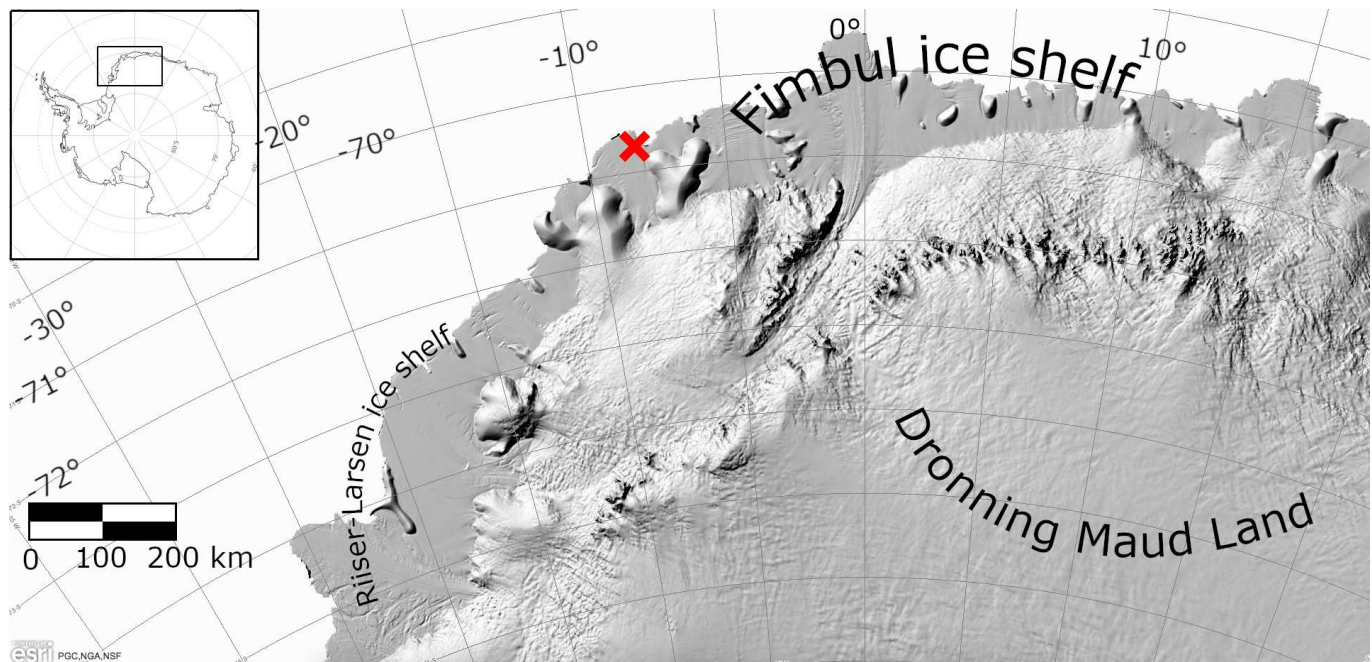


Figure 1. Map of the Antarctic continent, the red cross indicates the location of Neumayer Station. Imagery (C) 2016 DigitalGlobe, Inc.

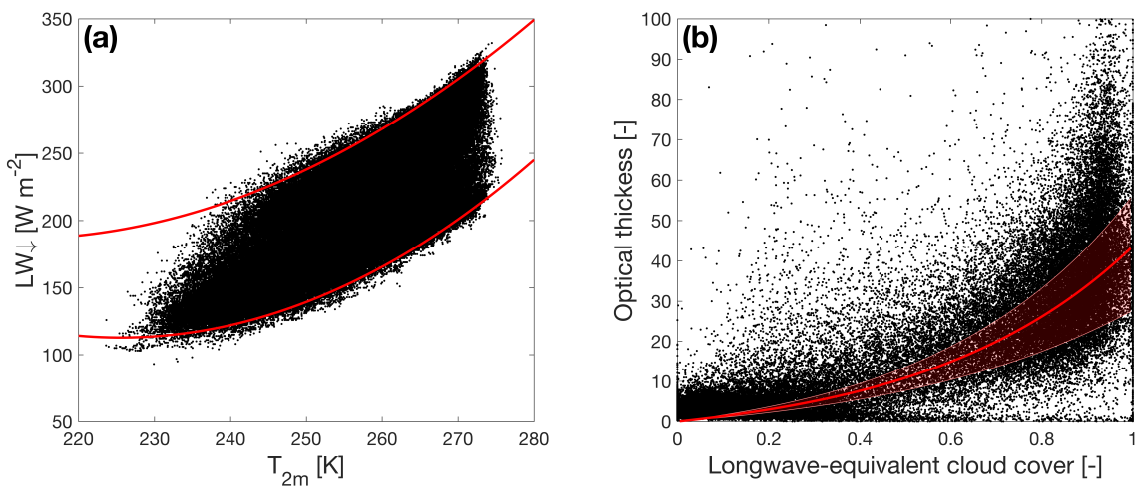


Figure 2. (a) Downward longwave radiation versus air temperature. The red lines are quadratic fits of the upper and lower 5 percentile boundaries. The longwave-equivalent cloud cover is determined by linear interpolation between these bounds. (b) Optical thickness versus cloud cover. The red line resembles the best fit to a function $\tau = c_1 (e^{c_2 N_e} - 1)$, the shaded area indicates the 95% uncertainty range.



Table 1. Listing of used measurement variables and their associated measurement errors.

Variable	Neumayer errors
V_{10m}	max(0.5 m/s, 5%)
$SW \downarrow$	5 W/m ²
$SW \uparrow$	5 W/m ²
$LW \downarrow$	5 W/m ²
$LW \uparrow$	5 W/m ²
T_{2m}	0.1°C
RH_{2m}	5%
p	0.5 hPa

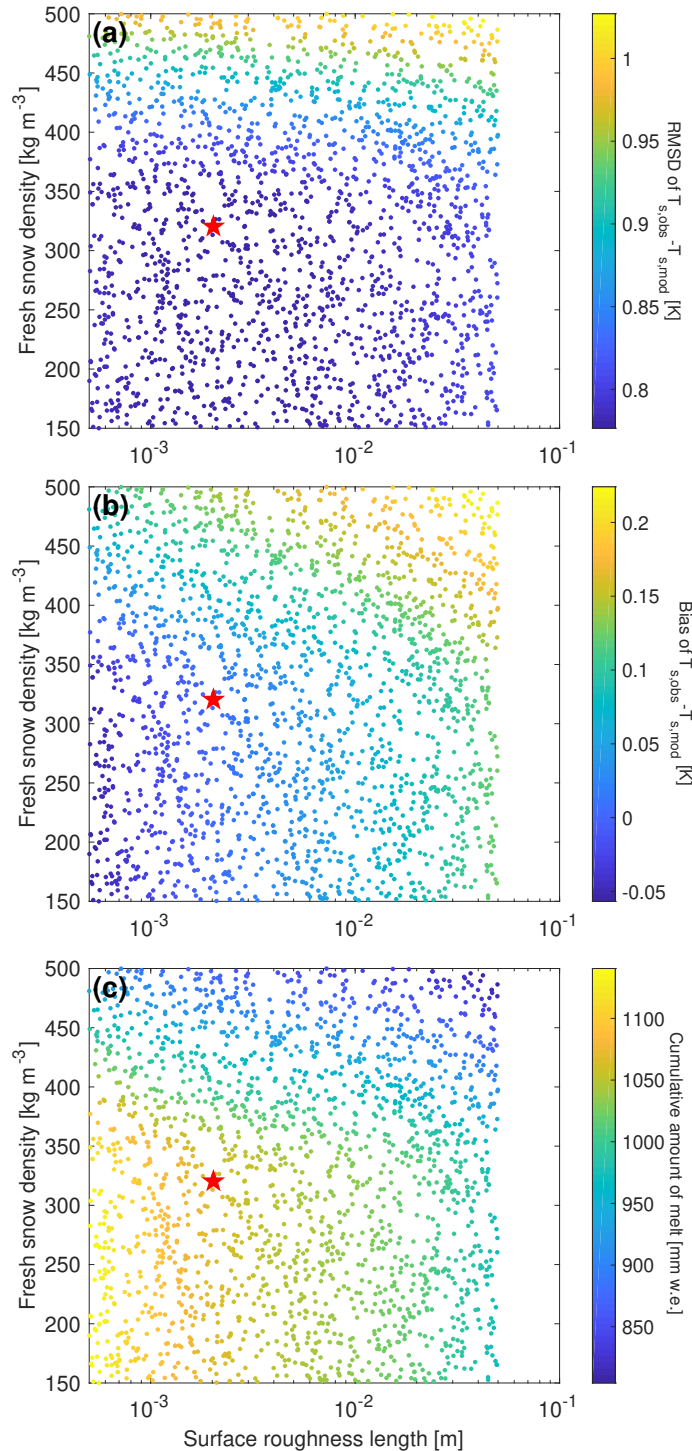


Figure 3. Lower limit of fresh snow density $\rho_{s,0}$ versus surface roughness length for momentum $z_{0,m}$ plot. Colour codes indicate **a)** the RMSD and **b)** bias of the observed versus modelled surface temperature (c.f. Fig. 4) and **c)** the cumulative amount of modelled melt. In all plots the red star indicates the value for which the RMSD of the comparison is the lowest.

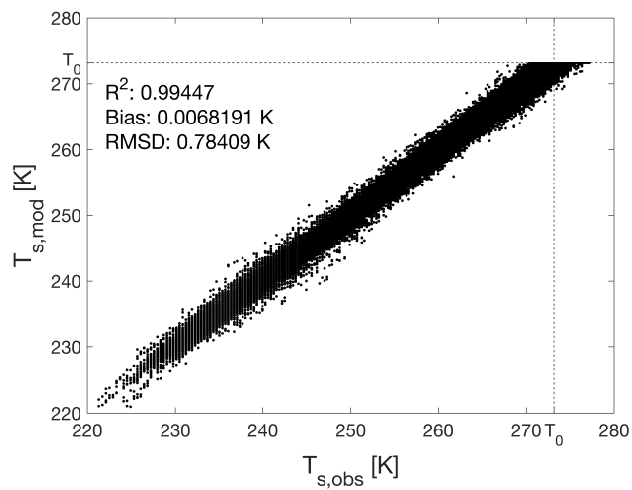


Figure 4. Daily values of modelled versus measured T_s for the parameter settings used in the remainder of this study: $z_{0,m} = 2$ mm, $\rho_{s,0} = 320 \text{ kgm}^{-3}$.

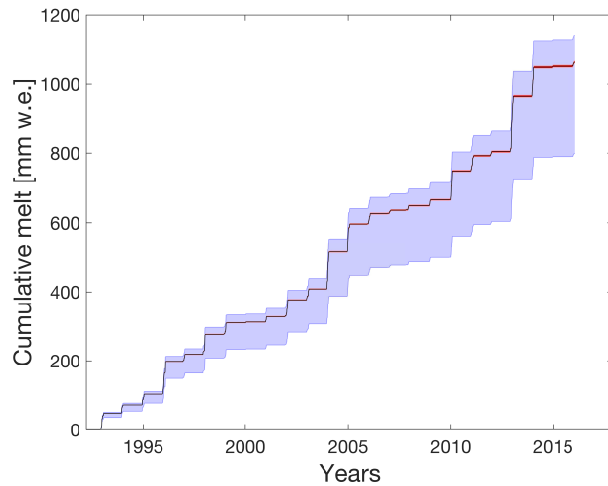


Figure 5. Effect of measurement and model uncertainties on cumulative melt. The shaded red area indicates the 1σ range due to measurement uncertainties, the shaded blue area indicates the range due to model uncertainties (changing $z_{0,m}$ and $\rho_{s,0}$ between their respective values). The latter uncertainty band is asymmetrical because the values that are used for the rest of the study ($z_{0,m} = 2$ mm, $\rho_{s,0} = 320 \text{ kg m}^{-3}$) are not in the middle of the range that was probed.

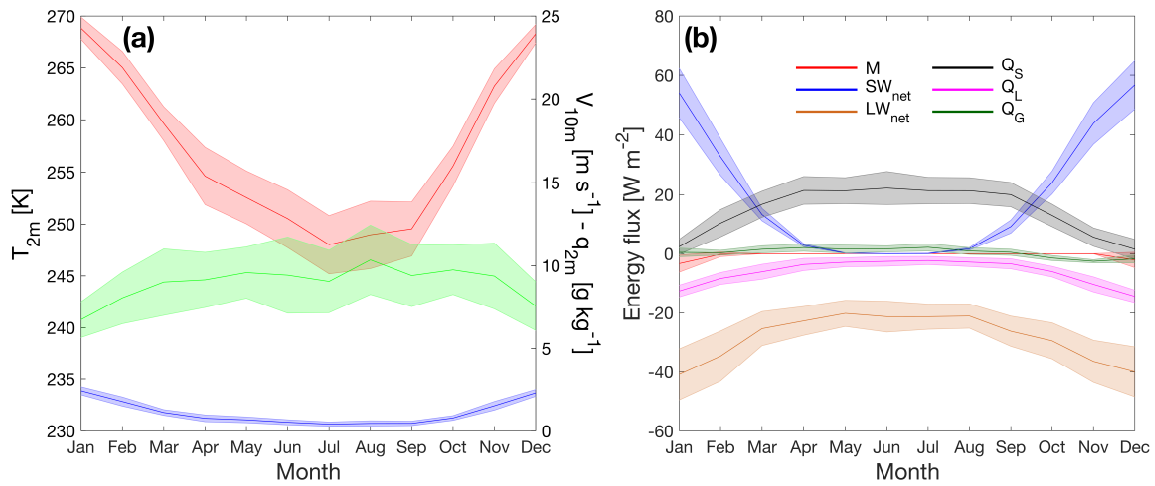


Figure 6. **a)** Seasonal cycles of temperature (red, left axis), 10 metre wind speed (green, right axis) and specific humidity (blue, right axis). Shaded areas indicate the standard deviations of monthly means. **b)** Same as **a)** for melt (red), net shortwave radiation (blue), net longwave radiation (orange), sensible heat (black), latent heat (magenta) and ground heat (green).

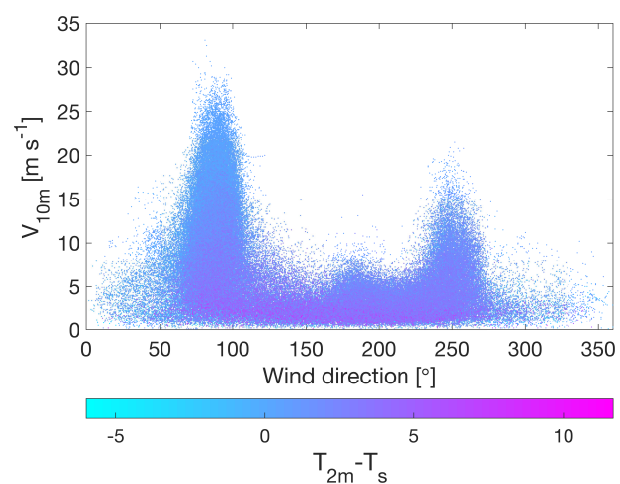


Figure 7. Wind speed as a function of wind direction. Colour codes indicate the temperature difference between the air T_{2m} and the surface T_0 .

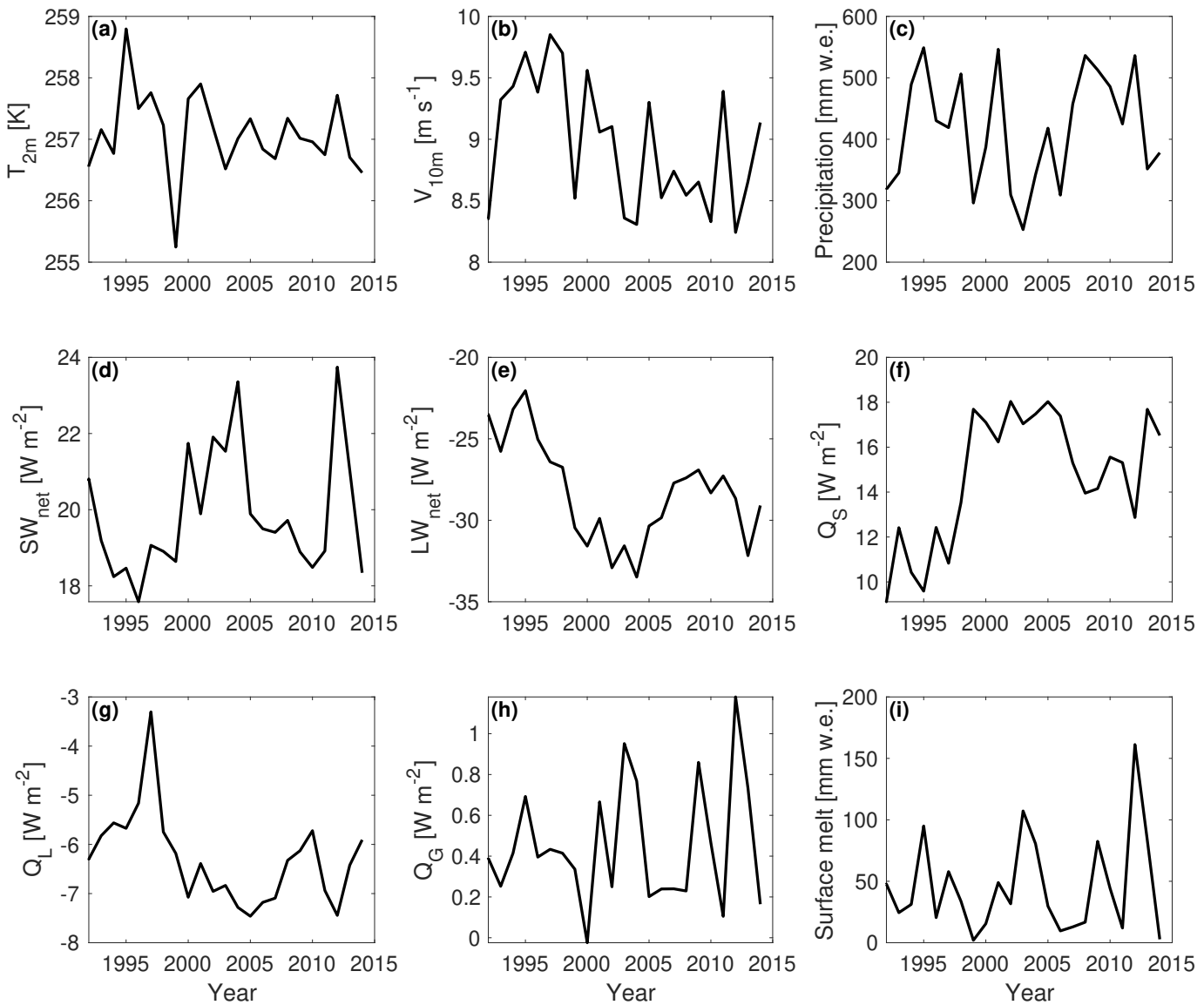


Figure 8. Time series of average annual values of **a)** 2-metre temperature, **b)** 10-metre wind speed, **c)** precipitation, **d)** net shortwave radiation, **e)** net longwave radiation, **f)** sensible heat flux, **g)** latent heat flux, **h)** ground heat flux and **i)** amount of melt for Neumayer.



Table 2. Mean annual values and interannual variability of meteorological variables and SEB components. For precipitation and melt, total annual values are given.

Variable	Yearly mean	Variability
T_{2m} (K)	257.1	0.7
T_s (K)	256.0	0.8
q_{2m} (g kg^{-1})	1.1	0.1
V_{10m} (m s^{-1})	9.0	0.5
p (hPa)	981.5	1.9
SW_{net} (W m^{-2})	20	2
$SW \downarrow$ (W m^{-2})	127	3
$SW \uparrow$ (W m^{-2})	107	2
LW_{net} (W m^{-2})	-28	3
$LW \downarrow$ (W m^{-2})	218	5
$LW \uparrow$ (W m^{-2})	246	4
Q_S (W m^{-2})	14.7	2.9
Q_L (W m^{-2})	-5.3	0.9
Q_G (W m^{-2})	0.5	0.3
Precipitation (mm w.e.)	418	91
Melt (mm w.e.)	46	40

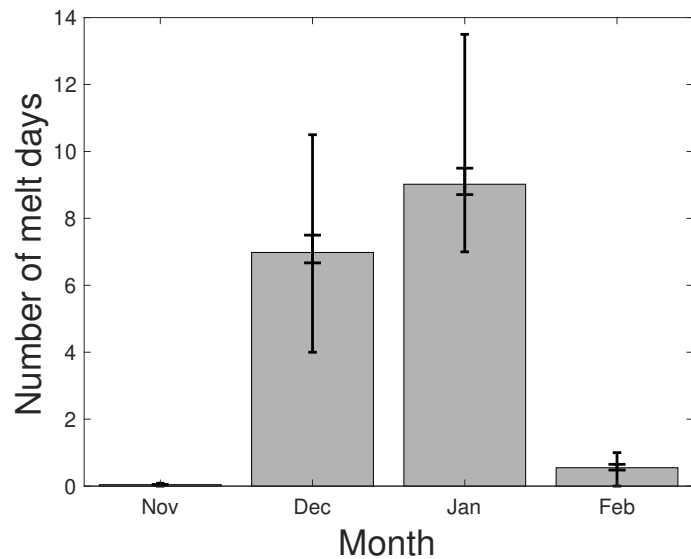


Figure 9. Average number of melt days per month at Neumayer. The inner error bars (with larger caps) indicate the 1σ uncertainty range resulting from the runs performed with different settings for roughness length z_0 and lower limit of fresh snow density $\rho_{s,0}$ (Sect. 3.1). The outer error bars (with smaller caps) indicate the 1σ range of the interannual variability.

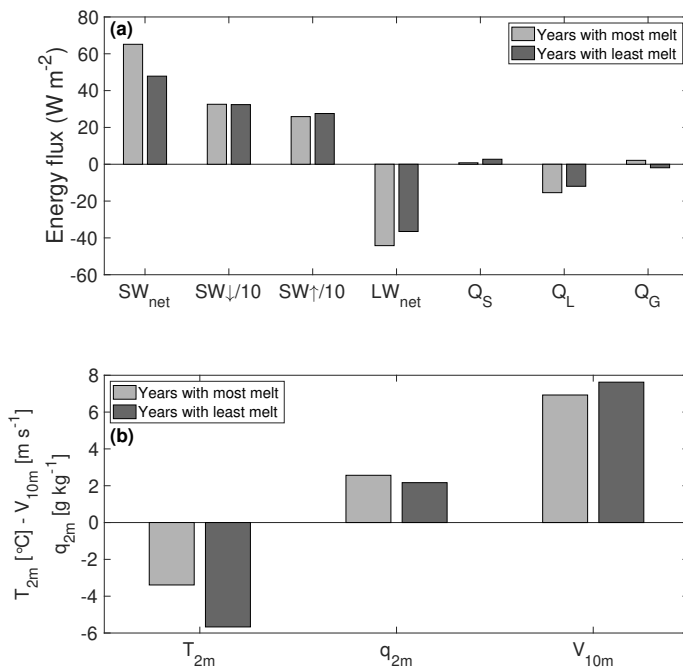


Figure 10. Average values of **a)** some SEB components and **b)** some meteorological variables for December and January in the years with the highest (light grey) and lowest (dark grey) amount of melt, as identified in Sect. 3.4. Note that $SW \downarrow$ and $SW \uparrow$ are scaled by a factor of 10 in **a)** for clarification.

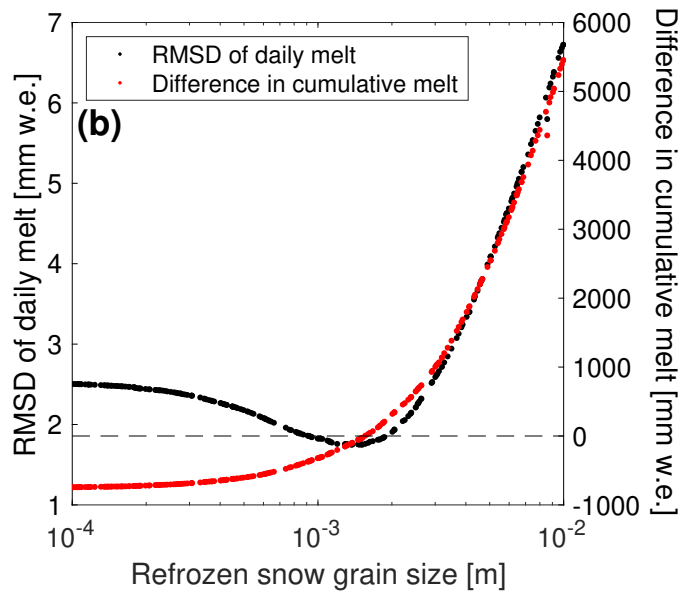
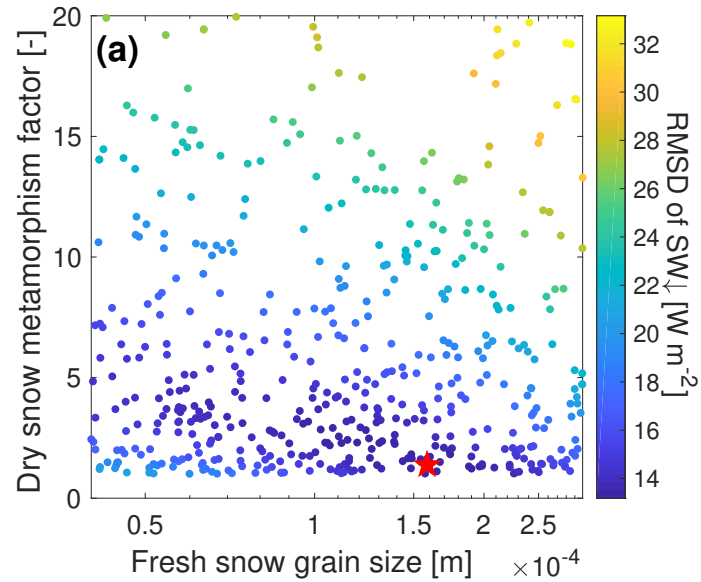


Figure 11. **a)** Dry snow metamorphism factor versus fresh snow grain size ($r_{e,0}$). The colours indicate the RMSD of the evaluation of the incoming shortwave radiation during the dry season, i.e. from the first day that the Sun rises more than 15° above the horizon, until the first day that surface melt occurs. For all runs, a different value for $r_{e,0}$ and the dry snow metamorphism factor are taken. The red star indicates the location of lowest RMSD. **b)** RMSD of daily melt (black, left axis) and difference in cumulative melt (red, right axis) as a function of refrozen snow grain size ($r_{e,r}$). The value that is used for the rest of the study is the one for which the difference in cumulative melt is closest to zero (dashed black line).

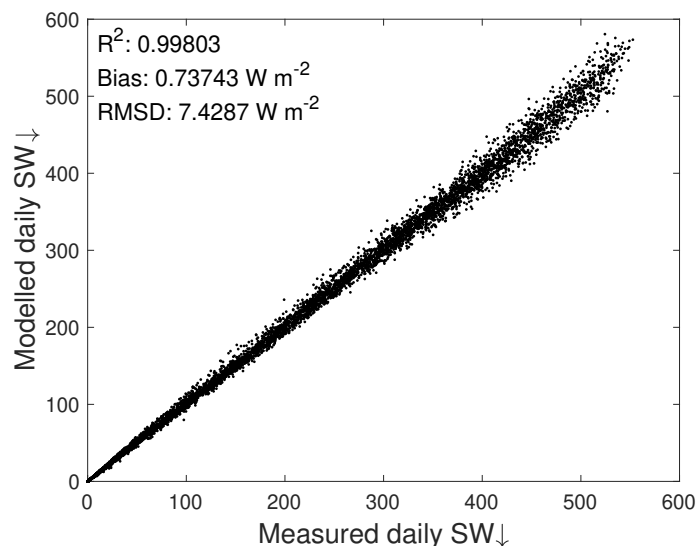


Figure 12. Measured versus modelled daily average incoming shortwave radiation ($SW \downarrow$). The modelled $SW \downarrow$ was obtained by dividing the hourly measured $SW \uparrow$ by the calculated hourly albedo.

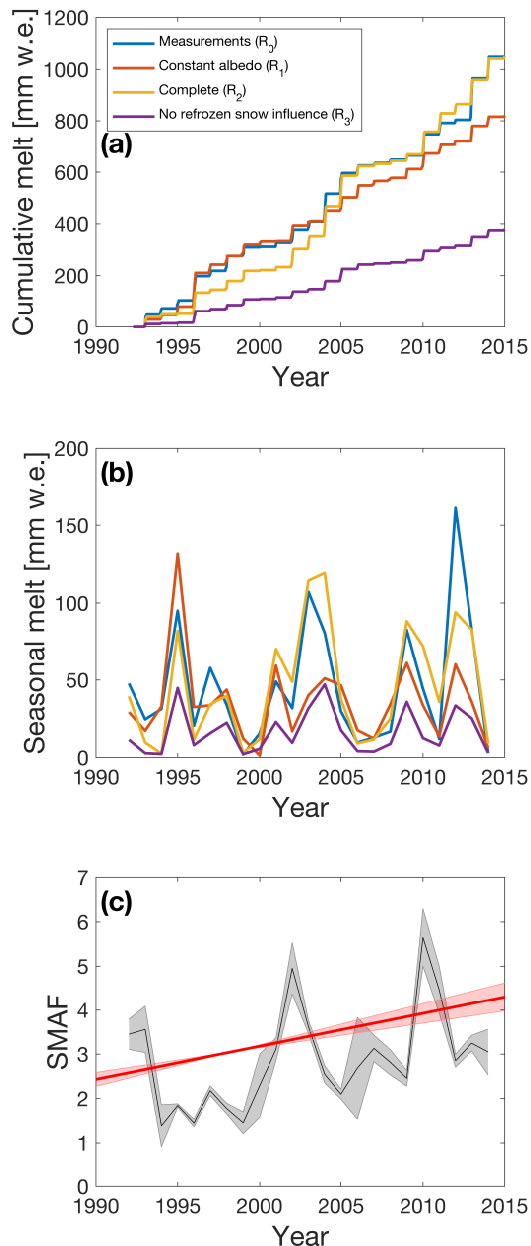


Figure 13. **a)** Timeseries of cumulative amount of melt for the run with measured albedo (R_0 , blue), a constant albedo of 0.84 (R_1 , red), a run in which refrozen snow does impact snow grain size (R_2 , yellow) and a run in which snow grain size is not influenced by refrozen snow (R_3 , purple). **b)** Same as **a)** but for seasonal amount of melt. **c)** Ratio of modelled surface melt between yellow and purple lines in **a)** and **b)** (runs R_2 and R_3 respectively). The grey area indicates the uncertainty coming from the uncertainty in the determination of τ (Fig. 2b)) and $\pm 5 \text{ W m}^{-2}$ measurement uncertainty in incoming shortwave radiation. The red line represents the best least squares fit, the shaded area indicates the 95% confidence limits on this fit.